Analytical 'steady-state'-based derivation and clarification of the courant-friedrichs-lewy condition for pipe flow

Zdzisław Kowalczuk [*], Marek Sylwester Tatara

Department of Robotics and Decision System, Faculty of Electronics, Telecommunications and Informatics, Gdańsk University of Technology, Ul. Narutowicza 11/12, 80-233, Gdańsk, Poland

ARTICLE INFO

ABSTRACT

This article addresses the problem of choosing the optimal discretization grid for emulating fluid flow through a pipeline. The aggregated basic flow model is linearized near the operating point obtained from the steady state analytic solution of the differential equations under consideration. Based on this model, the relationship between the Courant number (μ) and the stability margin is examined. The numerically set coefficient μ_{opt}, ensuring the maximum margin of stability, is analyzed in terms of the physical and technological parameters of the flow. As a result of this analysis, a specific formula is obtained based on parameters describing the mechanics (geometry and physics) of the flow through the pipeline, which leads to the optimal value of the Courant number, separately for smooth and rough pumping conditions. A more detailed analysis of the distribution of the optimal μ coefficient in relation to the parameters of the pipeline flow mechanics shows four cases to consider when determining the coefficient μ_{opt}. Surprisingly, in three cases, the CFL condition is insufficient, which is expressed in the form of the proposed procedure for choosing the optimal value of μ. The final dichotomous model is derived from the Monte Carlo simulation results in which the effect of each parameter on the optimal Courant number is estimated and consolidated. Taking into account the recognized general laws of physics and using numerical methods and mathematical analysis, simple and useful analytical relationships describing the flow process are obtained. In addition, computer simulations are performed to verify the correctness of the proposed procedure, as well as a number of other considerations related to the modeling of fluid flow in transport pipelines.

1. Introduction

Numerical stability plays an important role in many engineering disciplines, including finding computational solutions for partial differential equations and emulating[1] processes in the real world, where it is required to match numerical models to the analyzed process (Kowalczuk and Tatara, 2018, 2020). Stability is extremely important because it determines the correct operation of systems and the consistency of results. The issue of flow model stability is closely related to the physical parameters of this process, the chosen discretization grid and the implemented discretization scheme. It is usually assumed that the physical parameters of the analyzed process are constant and remain unchanged during emulation. Similarly, the discretization scheme is selected before implementation. The discretization grid is also chosen by the system designer (according to certain criteria), and can be adaptively changed while the solution is being calculated.

There are methods to help you choose the appropriate discretization. The early Lax Equivalence theorem (Lax and Richtmyer, 1956) indicated that a consistent linear numerical scheme with well-set initial conditions converges if and only if it is stable. Hence the importance of theoretically grounded stability (Thomas, 1995) that underpins systems engineering.

One of the most recognizable selection methods is the Courant-Friedrichs-Lewy (CFL) principle, which specifies the condition necessary for the convergence of the difference equation approximating the partial differential equation (Courant et al., 1967). For many years, researchers have been referring to this condition when performing simulations (Woodward and Colella, 1984; Bauer et al., 2008; Thanh, 2014; Kornhaas et al., 2015; Duquette et al., 2016; Capuano et al., 2017; Yeung et al., 2018; Wang et al., 2018; Shao and Li, 2018; Decuyper et al., 2018; Hafsi et al., 2019; Alghurabi et al., 2020). The CFL criterion is not only

---

* Corresponding author.
E-mail addresses: kova@pg.edu.pl (Z. Kowalczuk), marek.tatara@pg.edu.pl (M.S. Tatara).
[1] Emulation means real-time simulation. The term here refers to a situation where a numerical model is instantiated in the final application, where (on-line) measurements are collected in real time and entered into the system implementing the model.

essential in the field of computational fluid dynamics, but is also considered paramount in other sciences, for example in antenna physics and electromagnetic field theory (Namiki and Ito, 1999; Chen and Zhang, 2001). Schemes seemingly not requiring compliance with the CFL principle are also proposed, but then usually other or equivalent singularities appear that limit the rationality or computability of the result (Namiki and Ito, 1999; Chen and Zhang, 2001; Stefański and Drysdale, 2008; Czernous, 2008; Kowalczuk et al., 2018). The basic starting point is practical knowledge related to the Courant-Friedrichs-Lewy condition, which limits and binds the discretization steps, without closing the possibility of further optimization (*e.g.* by trial and error). The problem of optimal selection of the discretization grid is therefore an extremely important issue in numerics, calculations and simulations (you can also refer to publications (Gordner and Wittum, 2007; Kowalczuk and Tatara, 2016)).

Model-based approaches to pipeline flow diagnostics are based on flow process emulation that enables comparative analysis of actual measurements. The crucial point of such calculations is the numerical stability of the emulated model (Kowalczuk and Tatara, 2016). This means that the choice of discretization grid should be given special attention.

The main contribution of this article is the method of choosing optimal steps in space and time. It was achieved by analyzing the impact of various factors and physical parameters of the flow process on the sought solution. In particular, the optimal choice of steps should be understood in terms of maximizing the margin of system stability (in the classical sense). The intended consequence of such approach is the relative robustness of the numerical algorithm for the uncertainties in the model, as well as – due to related complex non-linear relationships – insensitivity to measurement variation or deviation. When thinking about emulation processes, you can use a pseudo-time stepping approach, in which, at each stage, the time step can be locally optimized using the proposed formula. Due to real-time computation constraints (imposed by limited field computer resources), the time step should always be determined safely and instantaneously. Often, some process parameters are previously unknown or may change during implementation or the emulation itself. Therefore, the time step cannot be predetermined and must be calculated in real-time. Due to the large number of possibilities, it also cannot be taken from a look-up table. Thanks to the main result of this work, concerning the formula for choosing the optimal method of discretization, you will not have to guess the correct value of the steps by trial and error, as in the case of the Courant-Friedrichs-Lewy condition. Instead, assuming that the current parameters are estimated correctly, and using the classic principle of certainty equivalence (a more detailed discussion of this issue is provided in Appendix B), we are able to calculate the optimal discretization grid.

In practice, the appearance of unforeseen operational situations may cause that the applied solution will work in other conditions than those for which it was technically adjusted. Such cases are widely known in engineering and can also cause various 'lethal' side effects in terms of theoretical-mathematical, numerical-computational and practical implementation. On the other hand, there are no better methods than computer ones. Therefore, although numerically difficult, the problem considered here is extremely important. It is worth mentioning the recent work of (Konangi et al., 2018) on a similar problem and analyzing the stability ranges as a function of Mach number. In contrast, we analyze (i) the *optimal* Courant number as (ii) a *multivariate* function of the physical coefficients of the pipeline.

It is thus well known that due to the existing numerical problems, an attempt to implement a model in practice may lead to "overloading" or preventing its computer implementation. In some cases, shared engineering experience may lead to the empirical discovery of specific requirements (such as the CFL principle) and the emergence of various interesting theoretical problems that are always worth expressing in a rigorous mathematical framework.

From a theoretical and practical point of view, our analysis leads to an interesting categorization, in which we take into account geometric, physical, technological, mathematical and numerical parameters. The obtained classification, together with apt mathematical modeling, allows us to provide analytical formulas explaining the phenomena related to the CFL principle, and the issue of the optimal Courant number and optimal discretization grid, and as a result leads to a well-conditioned simulation/emulation.

Let us consider purely practical and engineering aspects. As mentioned, the optimal Δt can be variable over time (at any stage), improperly selected parameters can easily destabilize the system, and a simple approach to this problem (*e.g.* trial and error method) may be unacceptable (*e.g.* from a technological point of view). In addition, the target system environment may not be available to the operator. Therefore, the practical goal of this development is to determine the feasibility conditions for automating the process of choosing the time and space step.

2. Discretization of the base model

Considering the intention to solve the target problem of choosing the optimal discretization grid suitable in emulation of the pipeline flow process, which is, for example, part of a field-deployable leak detection and isolation system, we will start with a continuous mathematical formulation of the analyzed process.

The continuous-time model of the flow process can be derived from the laws of conservation of mass and momentum. As a result, through some simplifications, assuming an isothermal incompressible flow, the following two partial differential equations can be given (Billmann and Isermann, 1987; Kowalczuk and Tatara, 2020):

$$\frac{S}{\nu^2}\frac{\partial p}{\partial t} + \frac{\partial q}{\partial z} = 0 \tag{1}$$

$$\frac{1}{S}\frac{\partial q}{\partial t} + \frac{\partial p}{\partial z} = -\frac{\lambda \nu^2}{2DS^2}\frac{q|q|}{p} - \frac{g \sin \alpha}{\nu^2}p \tag{2}$$

where S is the cross-sectional area [m^2], ν is a surrogate speed of sound in the fluid [$\frac{m}{s}$], D is the diameter of the pipe [m], q is the mass flow [$\frac{kg}{s}$], p is the pressure [Pa], t is the time [s], z is the spatial coordinate [m], λ is the generalized dimensionless friction coefficient,[2] α is the inclination angle [rad], and g is the gravitational acceleration [$\frac{m}{s^2}$]. The surrogate speed of sound, which is a quantity related to the isothermal speed of sound, can be calculated as

$$\nu = \sqrt{\frac{p}{\rho}} \tag{3}$$

where ρ is the density of the fluid.[3] Since the question of the applicability of such a surrogate is quite complex, you can refer to the discussion in (Kowalczuk and Tatara, 2020).

The model of Eqs. (1) and (2) was derived with the assumptions of a constant pipe diameter and operation in turbulent flow region ($Re > 4000$). In addition, the elastic effects of walls are neglected, the speed of sound is constant, and the velocity of flow is significantly smaller than the speed of sound. We also assume that the considered pipe is 'long' (Billmann and Isermann, 1987). Such a description is subject to discretization by means of finite low-order differential schemes (Billmann and Isermann, 1987):

$$\frac{\partial x}{\partial t} = \frac{3x_n^{k+1} - 4x_n^k + x_n^{k-1}}{2\Delta t} \tag{4}$$

---

[2] The Darcy friction factor (White, 2011; Kowalczuk and Tatara, 2020).

[3] We can also briefly refer to Eq. (3) as the speed of sound.

Z. Kowalczuk and M.S. Tatara

Journal of Natural Gas Science and Engineering 91 (2021) 103953

MOST WIEDZY Downloaded from mostwiedzy.pl

$$\frac{\partial x}{\partial z} = \frac{x_{n+1}^{k+1} - x_{n-1}^{k+1} + x_{n+1}^{k} - x_{n-1}^{k}}{4\Delta z} \tag{5}$$

where Δz and Δt are, respectively, spatial and time steps. The subscript indicates the segment index of the pipe, and the superscript is the discrete-time step number. It is assumed, as shown in Fig. 1, that the pressures are estimated and monitored at the end of the odd pipeline segments, while the flow rates at the end of the even sections. In the considered case of dynamic flows, in order to determine successive pressures and mass flows, we need to know the adjacent mass flows and pressures. It is important that pressure and flow measurements are only available at (both) pipe ends.

The discretization of the model Eq. (1)–Eq. (2) using schemes Eq. (4) and Eq. (5) leads to the following set of difference equations describing the pipeline flow process:

$$ap_n^{k+1} - b\left(q_{n-1}^{k+1} - q_{n+1}^{k+1}\right) = \frac{a}{3}\left(4p_n^k - p_n^{k-1}\right) + b\left(q_{n-1}^k - q_{n+1}^k\right) \tag{6}$$

$$b\left(p_{n+1}^{k+1} - p_{n-1}^{k+1}\right) + cq_n^{k+1} = b\left(p_{n-1}^k - p_{n+1}^k\right) + Y_n p_n^k + \left(\frac{4c}{3} + F_n^k\right)q_n^k - \frac{c}{3}q_n^{k-1} \tag{7}$$

with physical coefficients

$$a = \frac{3S}{2\nu^2\Delta t}, \ b = \frac{1}{4\Delta z}, \ c = \frac{3}{2S\Delta t}, \ Y_n = -\frac{g\sin\alpha_n}{\nu^2} \tag{8}$$

$$F_n^k \simeq -\frac{\lambda\nu^2}{DS^2}\frac{|q_n^k|}{p_{n-1}^k + p_{n+1}^k} \tag{9}$$

where α_n denotes the inclination angle of the *n*-th segment. The approximation Eq. (9) results from presenting the central pressure p_n^k as the mean value of pressures from adjacent segments. The set of two equations Eq. (6) and Eq. (7) can be expressed in the form of the following state-space model:

$$\mathbf{A}\widehat{\mathbf{x}}^k = \mathbf{B}\widehat{\mathbf{x}}^{k-2} + \mathbf{C}(\widehat{\mathbf{x}}^{k-1})\widehat{\mathbf{x}}^{k-1} + \mathbf{D}\mathbf{u}^{k-1} + \mathbf{E}\mathbf{u}^k \tag{10}$$

where the state and input vectors are defined as

$$\widehat{\mathbf{x}}^k = \left[\widehat{q}_0^k\widehat{q}_2^k\widehat{q}_4^k\cdots\widehat{q}_N^k\widehat{p}_1^k\widehat{p}_3^k\widehat{p}_5^k\cdots\widehat{p}_{N-1}^k\right]^\top \in \mathbb{R}^{N+1}$$

and

$$\mathbf{u}^k = \begin{bmatrix} p_0^k & p_N^k \end{bmatrix}^\top \in \mathbb{R}^2$$

respectively (Gunawickrama, 2001). Symbols with hats indicate estimates.

The matrices $\mathbf{A}$, $\mathbf{B}$, $\mathbf{C}$, $\mathbf{D}$ and $\mathbf{E}$ (Kowalczuk and Tatara, 2017) are specifically described in Appendix A.

The form Eq. (10) shown above makes it difficult to analyze the numerical stability of the model. Since matrix $\mathbf{A}$ is proved to be invertible (Kowalczuk and Tatara, 2017), equation Eq. (10) can be rewritten in a nonsingular state-space form:

$$\widehat{\mathbf{x}}^k = \mathbf{A}^{-1}\left(\mathbf{B}\widehat{\mathbf{x}}^{k-2} + \mathbf{C}(\widehat{\mathbf{x}}^{k-1})\widehat{\mathbf{x}}^{k-1} + \mathbf{D}\mathbf{u}^{k-1} + \mathbf{E}\mathbf{u}^k\right) \tag{11}$$

Recalling the results presented in Kowalczuk and Tatara (2017), an aggregated state vector $\widetilde{\mathbf{x}}^k = \left[\widehat{\mathbf{x}}^{k\top}\widehat{\mathbf{x}}^{k-1\top}\right]^\top$ and an aggregated input $\widetilde{\mathbf{u}}^k = \left[\mathbf{u}^{k\top}\mathbf{u}^{k-1\top}\right]^\top$ can be defined, which allows for a useful model of the flow
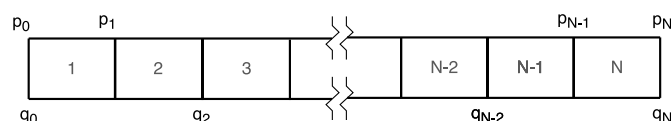
process to be shown as an aggregated dynamic equation in the state space, fitting a linear framework:

$$\widetilde{\mathbf{x}}^k = \mathbf{A}_c\widetilde{\mathbf{x}}^{k-1} + \mathbf{B}_c\widetilde{\mathbf{u}}^k \tag{12}$$

where

$$\mathbf{A}_c(\widetilde{\mathbf{x}}^{k-1}) = \begin{bmatrix} \mathbf{A}^{-1}\mathbf{C}(\widetilde{\mathbf{x}}^{k-1}) & \mathbf{A}^{-1}\mathbf{B} \\ \mathbf{I} & 0 \end{bmatrix} \tag{13}$$

$$\mathbf{B}_c = \begin{bmatrix} \mathbf{A}^{-1}\mathbf{E} & \mathbf{A}^{-1}\mathbf{D} \\ 0 & 0 \end{bmatrix} \tag{14}$$

Obviously, this is not full, but only apparent 'linearization', because matrix $\mathbf{A}_c$ is a function of the state vector $\widetilde{\mathbf{x}}^{k-1}$. Moreover, the $\mathbf{B}_c$ matrix strongly depends on the friction coefficient λ. When performing emulations, we calculate the $\mathbf{A}_c$ matrix in an iterative way, which means that we are dealing here with non-linear and variant (non-stationary) processing. Importantly, model Eq. (12) has a convenient form of state equations that can be analyzed using suitable numerical tools. Since non-linear effects associated with flow and pressure variables are present in Eq. (2), standard methods of linear stability analysis (*e.g.* von Neumann or frequency analysis Morton and Mayers (2005)) cannot be used here.

In order to guarantee the stability of the numerical system, the authors of Courant et al. (1967) recommend that the evaluation rate of the considered phenomenon be greater than the propagation velocity of the analyzed phenomenon (which is similar to the consequences of the famous sampling theorem). In its original version, the CFL rule states that the domain of numerical relation must cover the domain of analytical dependence.

This means that the discretization grid $\frac{\Delta z}{\Delta t}$ must be greater than or equal to the rate of information exchange in the appropriate differential equations (which is also called the characteristic method) for the computational system to be stable Bridson (2015). It turns out, however, that the CFL condition is only a necessary condition, which in general may turn out to be insufficient (it only gives the lower bound of the expression $\frac{\Delta z}{\Delta t}$, see also discussion in Appendix C).

In order to perform stable emulation, an appropriate discretization grid must be established. In particular, since the sound velocity ν is the highest transfer rate present in the flow process, the following inequality limitation (CFL) arises:

$$\frac{\Delta z}{\Delta t} \geq \nu \tag{15}$$

Moreover, by transforming the above into an equivalent equality form, the CFL condition can be expressed as:

$$\Delta t = \mu\frac{\Delta z}{\nu} \tag{16}$$

where μ is a coefficient from the range $\langle 0, 1 \rangle$ linking the two discretization steps, commonly called the Courant number.

In such a situation, a useful mesh parameter (m_h) of the analyzed discretization grid can be defined as:

$$m_h = \frac{\Delta z}{\Delta t} = \frac{\nu}{\mu} \tag{17}$$

The proposed discretization conditions are discussed in Appendix C, where the full grid visualization is presented. Our experience shows that for each set of technological parameters, there is a specific relationship between the quantization of time and space that guarantees a maximum margin of stability m. For the discrete models, this margin is measured as $m = 1 - s_{max}$, where s_{max} is the largest modulus of all eigenvalues of the state matrix $\mathbf{A}_c$ (Brogan, 1991).

Fig. 1. Spatial discretization grid of the pipeline.

3

3. Steady state evaluation leading to a linear model

Simulation experiments were performed for a number of pipeline diameters. The results are summarized in Fig. 2, where the stability margin is expressed as a function of the μ coefficient. When analyzing such plots for various sets of pipeline physical parameters, it was noticed that there is an exact value of this coefficient which leads to the maximum margin of stability of the analyzed numerical scheme.

The results shown in Fig. 2 were obtained with a considerable computational effort (20,000 iterations for each simulation experiment). However, it served to accurately determine the steady state. To determine whether a steady state was reached, two subsequent state vectors were compared. When the second norm of the resulting deviation vector is lower than the numerical noise level, it is assumed that the steady state conditions are satisfied.

Clearly, transient processes may cause difficulties in selecting the discretization grid. It is worth noting that these processes are also usually useless from the point of view of monitoring and diagnostics. Transient processes are also unreliable due to the differences between the real flow process and the numerical process as they include variations and fluctuations due to numerical effects (alien to the real world). That is why we weed the steady state, which is fully representative. It is also important that we were able to develop a precise steady-state formula (Kowalczuk and Tatara, 2020). All this will allow us to determine the appropriate model of the coefficient μ.

To emphasize the fact that the only pressures that are relevant from a practical point of view are those at the inlet and outlet of the pipe, we denote them as p_i and p_o, corresponding to p_0 and p_N, respectively.

Nonlinear differential equations require great computational effort to preserve stability, which is why, in many cases, the linearization around the known operating point is a standard procedure that reduces the complexity of the problem.

To implement the linearization procedure, we suggest moving from the numerical domain to the analytical field, in which we have achieved, *inter alia*, an analytical result (Kowalczuk and Tatara, 2018, 2020) regarding the method of calculating the steady state, which will be the basis of the linearization. In this way, we can provide an analytical solution of partial differential equations Eq. (1) and Eq. (2) in the steady state in the following form:

$$q = \text{sign}\left(p_i^2 - p_o^2\right)\sqrt{\left|\frac{DS^2}{\lambda\nu^2}\frac{p_i^2 - p_o^2}{L}\right|} \tag{18}$$
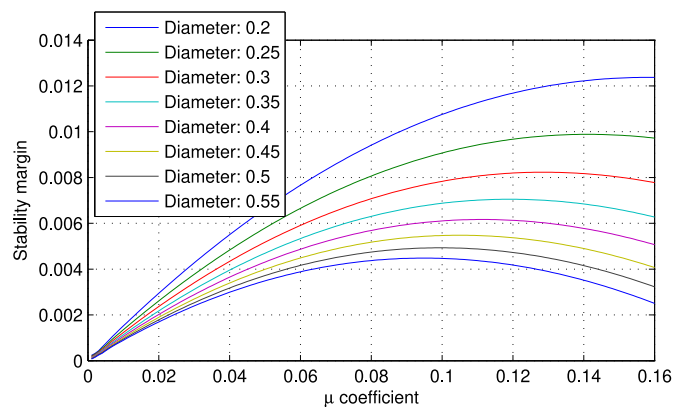
Fig. 2. Stability margin as a function of the μ coefficient for different diameters of a pipeline. Stability margin was measured after 20,000 iterations of the simulation algorithm. The other physical parameters of the pipeline were: $N = 10$, $L = 4000$ [m], $\lambda = 0.01$, $\nu = 304\ [\frac{m}{s}]$, $p_i = 32$ [bar], $p_o = 30$ [bar], and $\alpha = 0$ [°] (Kowalczuk and Tatara, 2016).

$$p = \sqrt{p_i^2 - z\frac{p_i^2 - p_o^2}{L}} \tag{19}$$

for a zero inclination (tilt) angle ($\alpha = 0$) and:

$$q = \sqrt{\left|\frac{2DS^2}{\lambda\nu^2}\frac{g\sin\alpha}{\nu^2}\left(\frac{p_i^2 - p_o^2 e^{2\frac{g\sin\alpha}{\nu^2}L}}{e^{2\frac{g\sin\alpha}{\nu^2}L} - 1}\right)\right|}\cdot\text{sign}\left(p_i^2 - p_o^2 e^{2\frac{g\sin\alpha}{\nu^2}L}\right) \tag{20}$$

$$p^2 = e^{-2\frac{g\sin\alpha}{\nu^2}z}p_i^2 + \left(\frac{p_i^2 - p_o^2 e^{2\frac{g\sin\alpha}{\nu^2}L}}{e^{2\frac{g\sin\alpha}{\nu^2}L} - 1}\right)\left(e^{-2\frac{g\sin\alpha}{\nu^2}z} - 1\right) \tag{21}$$

for a non-zero inclination angle, where z is a spatial coordinate.[4]

As shown above, the space-state model Eq. (12), although essentially non-linear, has a linear form of state-space equations. This model can now be (fully) linearized (you can call it the second stage of 'linearization') around the appropriate working point (Kowalczuk and Tatara, 2020), which in our case is a state vector consisting of the determined steady-state values of pressure and flow shown above. Note that the coefficient of friction is also required to calculate the flow rates Eq. (18) and Eq. (20), and therefore it must be estimated first (Kowalczuk and Tatara, 2020). A fixed-value state transition matrix is obtained by simply substituting the calculated steady state $\check{\mathbf{x}}$ for $\widetilde{\mathbf{x}}^\infty$:

$$\overline{\mathbf{A}}_c = \mathbf{A}_c(\check{\mathbf{x}})\big|_{\mathbf{x} = \left[\check{\mathbf{q}}^\top \quad \check{\mathbf{p}}^\top \quad \check{\mathbf{q}}^\top \quad \check{\mathbf{p}}^\top\right]^\top} \tag{22}$$

The precise value of the steady state $\check{\mathbf{x}}$ can be calculated as follows. According to Eq. (18) or Eq. (20), we conclude that the constant value of the mass flow along the pipe is:

$$q_n = \text{const} = q \quad \text{for } n = 0, 2, 4, \ldots, N \tag{23}$$

And the discrete-in-space version of the pressure distribution according to formulae Eq. (19) and Eq. (21) is given as, respectively:

$$p_n = \sqrt{p_i^2 - \frac{p_i^2 - p_o^2}{L}\Delta z n} \quad \text{for } n = 1, 3, \ldots, N - 1 \tag{24}$$

and:

$$p_n = \sqrt{\frac{p_i^2 - p_o^2 e^{2\frac{g\sin\alpha}{\nu^2}L}}{1 - e^{2\frac{g\sin\alpha}{\nu^2}L}} + \left(p_i^2 - \frac{p_i^2 - p_o^2 e^{2\frac{g\sin\alpha}{\nu^2}L}}{1 - e^{2\frac{g\sin\alpha}{\nu^2}L}}\right)e^{-2\Delta z\frac{g\sin\alpha}{\nu^2}n}} \quad \text{for } n=1,3,\ldots,N-1 \tag{25}$$

Putting Eq. (22) in Eq. (12), we get the following fully linearized dynamic equation of an aggregated vector $\overline{\mathbf{x}}$:

$$\overline{\mathbf{x}}^k = \overline{\mathbf{A}}_c\overline{\mathbf{x}}^{k-1} + \mathbf{B}_c\widetilde{\mathbf{u}}^k \tag{26}$$

Knowing the value $\overline{\mathbf{x}}^k$, we are able to calculate the emulation output values, *i.e.* the mass inlet and outlet flow rates that can be further processed or compared to measurements for leak detection, for instance.

Commentary 1. The presented linearization means a great methodological simplification of the modeling and computation problem discussed here. It is important that the above steady state of the flow

---

[4] When presenting the above solutions for steady state, we assume that all parameters are known. In fact, the problem is more complex (Kowalczuk and Tatara, 2020); among others the friction coefficient depends on the instantaneous value of the flow velocity. Therefore, it can change in any emulation step, and analytical solutions may differ from the true steady state. Thus they should be treated rather as an initial guess, taking into account current parameter values.

process is calculated analytically, based on the original partial differential equations of the flow process. Moreover, it should be noted that due to the linearization of the state transition matrix, the nonlinear effects of the pertinent parameters (q and p) become integrated into the state transition matrix (apart from the state itself).

Commentary 2. Although in general the results of simulations of various numerical (discrete-time) models that can be used in computer environments do not have to coincide with analytic solutions, relevant studies (Kowalczuk and Tatara, 2018) show that the steady-state vector obtained as a result of numerical simulation of the linearized model given by Eq. (26) converges in time to the analytic solution of the complete (continuous in space and time) flow process model (the higher the accuracy and complexity resulting from fine discretization, the better).

Commentary 3. The linearity effect obtained in Eq. (22), including the method Eq. (26) for calculating $\overline{\mathbf{A}}_c$ (see also Appendix D), allows us to perform a standard numerical stability analysis. Moreover, the model, together with the matrix $\mathbf{A}_c$, calculated for a given operating point allows us to predict both the state of the system and the output quantity (mass flow). The approach taken can be interpreted in terms of Certainty Equivalence (see Appendix B).

4. The largest possible margin of stability

In order to determine the optimal discretization mesh m_h or, equivalently, $\frac{\Delta z}{\Delta t}$, the linearized aggregated model Eq. (26) was simulated with a random choice of technological flow parameters, as presented in Table 1. Consequently, for each parameter set, the Courant number μ was optimized (yielding μ_{opt}) to ensure the highest possible margin of stability.

It is worth noting that our structure of the state space model covers only the technological parameters indicated in Table 1. While the influence of the flow rate is included in the computational parameters of the state transition matrix as well as in the state vector itself (compare also Appendix D).

Although the parameter ranges in Table 1 cover in practice the entire physically feasible search space, nevertheless the set of parameters used in the final application should be additionally checked in terms of meeting the assumptions and physical conditions of the base flow model (taking into account, for example, compressibility or incompressibility conditions, turbulent or laminar flows, etc.).

4.1. Preliminary analysis of the results obtained

At the beginning, each parameter was tested independently (with the other parameters fixed). However, since each simulation requires a long wait for a steady state (due to transient processes), the time required to collect the necessary data, especially for greater dimensionality of the model, was very long. In the linearized model, the state transition matrix is constant and the stability margin remains unchanged during simulation, therefore the time of data collection is significantly shortened. Note that the linearized model can be analyzed using classical systemic and mathematical tools, for example, the analysis of stability can be per-

Table 1
Range of parameters used for the simulation.

Parameter	Min	Max
Length L [m]	1	10^6
Diameter D [m]	0.001	2
Friction coefficient λ [-]	0.001	0.4
Number of segments N [-]	4	100
Inlet pressure p_i [Bar]	1	100
Outlet pressure p_o [Bar]	0.01	Inlet pressure
Surrogate sound velocity v [$\frac{m}{s}$]	250	2000

formed by determining the eigenvalues of the state transition matrix. This gives us the ability to run an optimization algorithm to find a curve in the $\Delta t - \Delta z$ plane that provides the maximum margin of stability:

$$m = 1 - s_{max} \qquad (27)$$

where s_{max} is the maximal absolute eigenvalue of the state transition matrix $\overline{\mathbf{A}}_c$.

For three exemplary pipeline lengths, a plot of the stability margin as a function of the Courant number was determined. This result is shown in Fig. 3 for a short pipe (100 km) case, in Fig. 4 you have the case of a medium pipe (1000 km), and Fig. 5 is for a long pipeline (5000 km).

In practice, we can recommend the use of $\mu = 1$, but only for some medium length pipes. Leaving a broader treatment of this topic for further research, we would like to limit ourselves here to the common (CFL) condition $\mu \leq 1$.

You can see that, for a short pipe (Fig. 3), the maximum stability margin is achieved at $\mu_{opt} \approx 0.36$, while the system becomes unstable at $\mu \approx 0.66$. The value of the μ coefficient for which the system becomes unstable will be called the critical Courant number μ_{crit}. It is thus clear that the CFL condition is not sufficient in the considered case and it is necessary to use a different method to specify μ_{opt}.

A similar situation can be observed for long pipes (Fig. 5), though the difference between μ_{opt} and μ_{crit} is much smaller ($\mu_{opt} = 0.993$, $\mu_{crit} = 0.936$). Again, we see that the optimal Courant number μ_{opt} should be specified very accurately.

Fig. 4 also requires some explanation. Based on purely mathematical considerations, one can come to the obvious conclusion that μ_{opt} is not restricted, and that the optimal stability margin can be found even with μ greater than 1 while maintaining system stability. In general, however, it should be noted that stability is not the only criterion for project rationality. With a set period Δt, sampling in space with a step Δz before the information arrives there does not seem rational, so according to CFL, you should use $\mu_{opt} \leq 1$. Otherwise, the state transition matrix is ill-conditioned and in general the flow process model does not meet the basic criteria for reliable modeling (repeatability). Therefore, below, all values of μ_{opt} greater than 1 will be truncated to 1.

5. Pipe description – factoring

After a detailed analysis of a wider range of experimental pipeline operating conditions (including various geometrical and physical parameters), we distinguish three basic classes (types) of pipeline technological operation (streaming, pumping) conditions as:
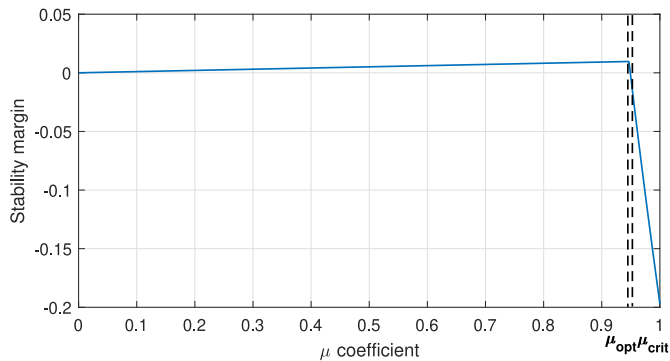
- rough,
- smooth,
- indefinite.
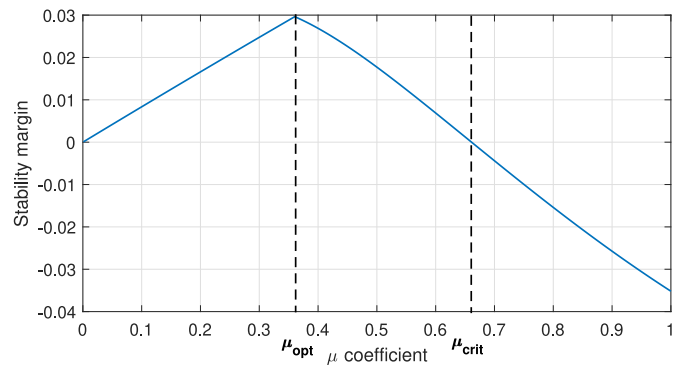
Fig. 3. Dependence of the stability margin on coefficient μ for a short pipe ($L = 100$ km). Assumed simulation parameters: $v = 1472$ [$\frac{m}{s}$], $D = 0.52$ [m], $\lambda = 0.0029$; $N = 16$; $p_i = 94.1$ [bar]; $p_o = 72.7$ [bar].
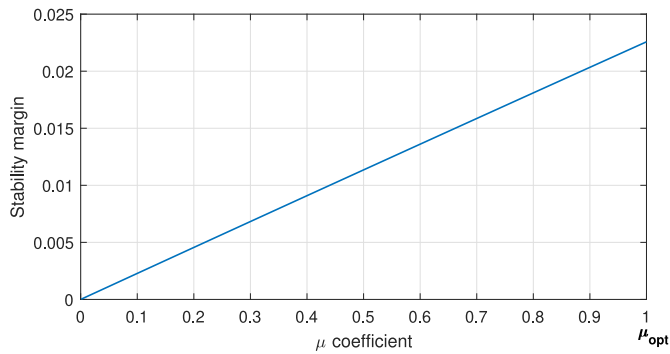
Fig. 4. Dependence of the stability margin on coefficient μ for a medium length pipe ($L = 1000$ km). Assumed simulation parameters: $\nu = 1472$ [$\frac{m}{s}$], $D = 0.52$ [m], $\lambda = 0.0029$; $N = 16$; $p_i = 94.1$ [bar]; $p_o = 72.7$ [bar].

Fig. 5. Dependence of the stability margin on coefficient μ for a long pipe ($L = 5000$ km). Assumed simulation parameters: $\nu = 1472$ [$\frac{m}{s}$], $D = 0.52$ [m], $\lambda = 0.0029$; $N = 16$; $p_i = 94.1$ [bar]; $p_o = 72.7$ [bar].

Rough and smooth conditions were identified as regions of pumping conditions, which, as we observed, can be identified using some simple indices (factors). The analysis of the impact of each parameter on the value of the optimal Courant number is summarized in Table 2. A deeper analysis shows that the relationship can be linear for some parameters, and quadratic for others. Positive means enlarging the value of μ_{opt} (and extending the space of useable μ). Therefore, to determine the optimal Courant number, we suggest the following development. Note also that as it results from our simulation study, the surrogate speed of sound has no effect on the optimal Courant number.

The observed dependencies of μ_{opt} on flow parameters show the dual, or even multiple, functionality of the Courant number. Originally, this factor was used for parameterization, stabilizing the discrete model. Now the ratio μ shows up as a precise tool in the feasibility study for system optimization (increasing the stability of the model).

Referring to the optimization issue, the optimal Courant number can be expressed in terms of purely mechanical properties of the pipeline

Table 2
Dependence of the optimal Courant number on the simulation parameters for two categories of pipe, showing the effects: (+) positive, (−) negative or (o) no relationship.

Parameter	Smooth conditions	Rough conditions
Length L [m]	(+)	(−)
Diameter D [m]	(−)	(+)
Friction coefficient λ [-]	(+)	(−)
Number of segments N [-]	(−)	(+)
Pressure drop $p_i - p_o$ [Bar]	(+)	(−)
Outlet pressure p_o [Bar]	(−)	(+)
Surrogate sound velocity ν [$\frac{m}{s}$]	(o)	(o)

system, which is the key conclusion of this report. In addition, thanks to the adopted differentiation of pipeline types, we can provide the exact formula for the optimal μ_{opt} (with reference to Table 2) for each of them. Consequently, our research shows that this solution can be described with one formula for μ_{opt}, which, due to its classification nature, will also be called the pipe factor Π:

$$\Pi = (\Pi_N)^i \vartheta_p \tag{28}$$

where $i = 1$ for smooth pumping conditions and $i = -1$ for rough pumping conditions, and the coefficients Π_N and ϑ_p are defined below. The value of the pipe factor, for cases where it is less than 1, can be associated with μ_{opt}. This means that the optimal Courant number can be computed directly using the given set of pipeline parameters.

Determining the mechanical factor of a pipe as:

$$\Pi_M = \sqrt{\frac{L\lambda}{D}} \tag{29}$$

which contains geometry (L, D) and physics (λ, constant generalized coefficient of friction) parameters, the aforementioned numerical ratio Π_N of the pipe can be shown as:

$$\Pi_N = \frac{1}{N}\Pi_M \tag{30}$$

without going into detail and before providing a specific classification, the μ_{opt} values obtained at constant inlet and outlet pressures for various pipeline numerical factors (Π_N) resulting from the change in pipe length L are shown in Fig. 6, where areas for smooth, rough and indefinite classes of conditions for pumping the medium through the pipeline have been marked.

Examining the plot of μ_{opt} versus the numerical pipe factor, we see two segments in the region of smooth operating conditions (at a point, the dependency of μ_{opt} on the pipe numerical factor does change) in Fig. 6. For safety, we will use a stronger limitation with respect to the coefficient μ_{opt} (preferring lower values). Indeed, in the middle (indefinite) region, the CFL condition is sufficient. In the case of higher values of the pipe numerical factor, a second region appears for which the CFL condition is not sufficient, and here too, a formula must be given to calculate the correct factor μ_{opt}. Interestingly, for long pipes, the value of μ_{opt} is inversely proportional to the numerical pipe factor.

Unfortunately, according to more detailed research, the numerical factor of the pipe is not sufficient to distinguish between the rough, smooth and indefinite classes of pumping conditions, which is why we have defined and used the following approximate dichotomous description of the pressure corrector ϑ_p in Eq. (28) for rough operating pipes:
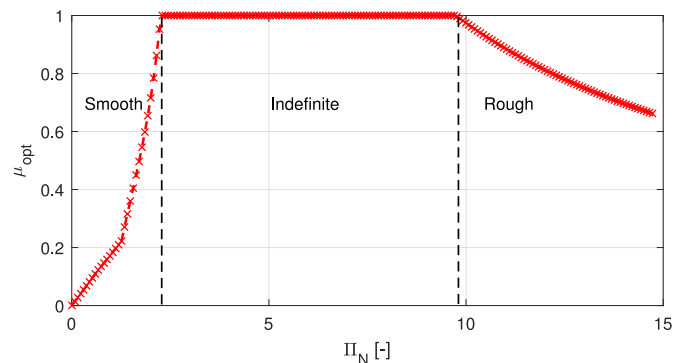
Fig. 6. Exemplary distribution of μ_{opt} in terms of the numerical pipeline factor Π^N controlled by changing the length of the pipe L (with the fixed parameters of the simulation: $\nu = 1472$ [$\frac{m}{s}$], $D = 0.52$ [m], $\lambda = 0.0029$; $N = 16$; $p_i = 94.1$ [bar]; $p_o = 72.7$ [bar]).

$$\vartheta_p^R = 8\sqrt{\frac{p_o^2}{p_i^2 - p_o^2}} \qquad (31)$$

and for smooth pumping conditions:

$$\vartheta_p^S = 0.5\sqrt{\frac{p_i - p_o}{p_i + p_o}} \qquad (32)$$

which introduces effects caused by pressure to Eq. (28). Note that the dichotomous corrector shows the explicit influence of pressures and the implicit effect of the pipe working conditions (smooth/rough). Another advantage of such parameterization is the logical separation of the effect of the geometry (N, L, D) and the technological and physical parameters (pressure and λ) in the common model of the Courant coefficient and pipe factor Eq. (28) for both cases $i = 1, -1$.

To cover the two (S/R) cases of Eq. (28), when the original CFL condition is not sufficient, we define the following condition (i) for rough operating conditions:

$$\Pi^R = \frac{1}{\Pi_N}\vartheta_p^R < 1 \quad \text{case}(i) \qquad (33)$$

and the corresponding condition (ii) for smooth conditions:

$$\Pi^S = \Pi_N \vartheta_p^S < 1 \quad \text{case}(ii) \qquad (34)$$

These two equations can also be equivalently rewritten as:

$$\vartheta_p^R < \Pi_N \qquad (35)$$

$$\Pi_N < \frac{1}{\vartheta_p^S} \qquad (36)$$

In view of the above, the developed formula Eq. (28), or equivalent set Eq. (33) and Eq. (34), receives a new interpretation and application as a technological classifier of pipelines. To a large extent, Eq. (28) can also be seen in practice as a balanced stream model. To sum up, formula Eq. (28) represents the common stream model, pipe factor, pipeline classifier and Courant number Eq. (28), for both (S/R) cases $i = 1, -1$.

Another advantage of the stream modeling based on the mechanical pipe coefficient, numerical factor and pressure corrector, relying on the applied parameterization, is the logical separation of the effects of the geometry (N, L, D) and physics (pressure and λ) in the common technological pipe factor Eq. (28), which allows, at the same time, the Courant number to be selected.

In addition, analyzing the impact of these parameters on the proposed mathematical formula Eq. (28), in particular Eq. (33) and Eq. (34), it can be easily concluded that there is a simple argument for the introduced concept of technological smoothness and roughness. On the one hand, the smoothness condition Eq. (34) can be improved by minimizing Π^S Eq. (34), Π_N Eq. (30) or ϑ_p^S Eq. (32), *i.e.* by reducing the pressure drop ($p_i - p_o$), L or λ, or by increasing the pressure (pressure head or p_{ref}(Kowalczuk and Tatara, 2020)), D or N. On the other hand, the roughness condition Eq. (33) is strengthened by minimizing Π^R Eq. (33) or ϑ_p^R Eq. (31) or by maximizing Π_N Eq. (30), *i.e.* by increasing the pressure drop ($p_i - p_o$) or pressure ratio (p_i/p_o) or L or λ or by reducing D or N. You can see that these actions are technically opposite to the case of striving for smoothness.

Because $\Delta z = L/N$, there is also a direct effect of L and N on the Courant number and the discretization grid. Thus, not only the relationship Eq. (17) between dz and dt matters, but also the absolute values of Δz and Δt. Therefore, these quantities should be used as a measure of the numerical scale of the pipe (pipe sections, pipe mesh and the pipe itself), *i.e.* as another numerical parameter with a significant effect on the pipe factor Π. All of these parameters relate to the model description of particular pipe sections (see also Appendix C).

As a result of the analysis from the previous paragraph, we can see that we need to add another parameter conditioning the categorization and digitization of the flow process. Namely, the improvement in smoothness Eq. (34) can be obtained by reducing the numerical scale of the pipe (Δz or Δt), and the strengthening of the roughness condition Eq. (33) can be achieved by increasing this scale.

Therefore, in short, and only taking into account mechanical and numerical considerations, smooth operating conditions characterize a relatively smooth surface, short and wide pipe sections, and small scale, while rough conditions - a relatively rough surface, long and narrow pipe sections, and large scale.

5.1. Additional comments

According to the results of the first approximate Monte Carlo numerical study described in Section 4 and the resulting observations of the value of the optimal coefficient μ_{opt} for various cases (related to numerical issues, pipe geometry and pressure control signals), the optimal Courant coefficient can be expressed in a simple (approximate) formula. In particular, the method of selecting the Courant number results from a mathematical description of the numerical results obtained (regarding smooth and rough conditions) during the first Monte Carlo computations, which consisted in analyzing the margin of stability in the adopted parameter space (pipeline length, diameter, friction coefficient, surrogate sound velocity in the medium, number of segments and pressure input and output).

Interestingly, the authors of (Hibbitt et al., 1979) noticed and distinguished the so-called slender pipes. While not all of the experimental conditions are reported, this type of pipe is consistent with our understanding of the rough operating conditions that include long and narrow pipelines. For example, the authors give approximate parameters of such pipes as follows: lengths $L \in [300 - 900]$ m (that is $1000 - 3000$ ft) and $D \in [0.1 - 0.25]$ m (or $4 - 10$ inches). Taking into account the limit values in such a situation, as well as the smallest considered value of the friction coefficient $\lambda = 0.001$, we obtain the range of the pipe mechanical coefficient as $\Pi_M \in [1, 2 - 9]$, which indicates our rough working condition (note that the inverse of Π_M is used when calculating the pipe factor for the rough conditions).

6. Factoring consequences and relations

It is worth emphasizing that the applied set of inequalities (Eq. (35) and (36)) should be considered in a holistic way to get the right result. If one of the above conditions is met, the working conditions should be qualified into one of these categories (smooth or rough). If none of these conditions are met, pipeline operating conditions are classified as indefinite, from now on referred to as the third case (iii).

Since we generally have two different pressure correction factors, ϑ_p^S and ϑ_p^R, we must also consider the composed case (iv) where both conditions are met simultaneously. As a consequence of the above, this situation can occur when the following condition is met:

$$\vartheta_p^R \vartheta_p^S < 1 \qquad (37)$$

By inserting values of the pressure corrector factors Eq. (31) and Eq. (32), one obtains:

$$4\sqrt{\frac{p_o^2}{p_i^2 - p_o^2} \frac{p_i - p_o}{p_i + p_o}} < 1 \qquad (38)$$

If this condition is met, then of course the situation is different from the indefinite one (neither smooth nor rough). Namely, smooth and rough areas intersect (have a common part). It also means that sometimes the pipeline operating conditions do not correspond individually to any of the three basic technology classes highlighted above.

Condition given by Eq. (38) can be rearranged as:

$$\sqrt{\frac{p_o^2}{(p_i - p_o)(p_i + p_o)}\frac{(p_i - p_o)}{(p_i + p_o)}} < 0.25 \tag{39}$$

$$\frac{p_o}{(p_i + p_o)} < 0.25 \tag{40}$$

to obtain a ratio of outlet to inlet pressure that fulfills the CFL exclusion condition:

$$\frac{p_o}{p_i} < \frac{1}{3} \quad \text{case} \quad (iv) \tag{41}$$

Interestingly, case (*iv*) can only occur if the pressure ratio is lower than the above threshold. Therefore, it turns out that the very analysis of the pressure ratio gives us an indication of whether or not the described complex case (*iv*) occurs.

Further analysis of the relationship between Π^R and Π^S shows that the feasible locations of pipelines on the Π^R–Π^S plane are hyperbolically bounded. This can be demonstrated as follows: By multiplying our two analytic pipe indicators (S/R), shown in Eq. (33) and Eq. (34), and using the above evaluations of the expression $\vartheta_p^R \vartheta_p^S$, we obtain the following relationship:

$$\Pi^R \Pi^S = \vartheta_p^R \vartheta_p^S = 4\frac{p_o}{(p_i + p_o)} \tag{42}$$

Since $p_o \in\; <0.01, p_i>$ (see Table 1), the right-hand side of Eq. (42) lies in the range $<0, 2>$. Therefore, the following holds: $0 \le \Pi^R \Pi^S \le 2$. Thus the 'pipe factors' relation on the Π^R–Π^S plane is bounded by the positive Π^R and Π^S axes and the following hyperbolic curve:

$$\Pi^R = \frac{2}{\Pi^S} \tag{43}$$

7. Final results

To select a specific value of μ_{opt}, we suggest the procedure in Fig. 7. First, check whether the condition of the pipeline in question can be classified as rough. If so, check if the pumping conditions also fall under the smooth conditions of the pipeline. If so, take $\mu_{opt} = \min\{\Pi^R, \Pi^S\}$. This is case (*iv*), where smooth and rough operating areas intersect and the pipeline's pumping conditions do not fall into only one of the two defined technological classes.[5] If the conditions are classified as rough, but not smooth, this is pure case (*i*) when $\mu_{opt} = \Pi^R$. A similar situation occurs when the pipeline conditions are classified as smooth, but not
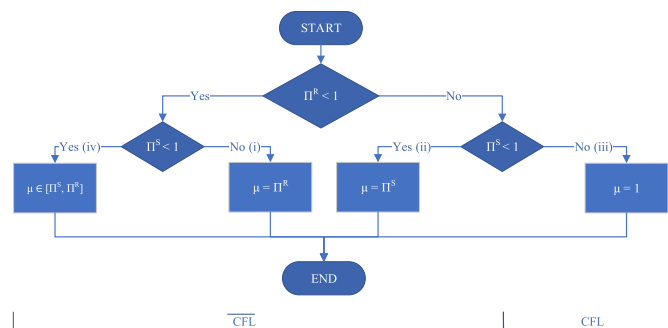
rough, and we have case (*ii*) and $\mu_{opt} = \Pi^S$. If the pipeline conditions under consideration cannot be classified as smooth or rough, we have case (*iii*) where **the CFL condition is sufficient**, *i.e.* $\mu_{opt} = 1$. The proposed method of determining the Courant number maximizes the chance that the system will be stable, even if the maximum stability margin is not reached.

8. Verification and secondary analysis - peculiarities and teasers

To verify the correctness of our result, we performed 1000 simulations with random parameters (within the ranges listed in Table 1). The distribution of the optimal stability margin in terms of the Π^S and Π^R functions, together with the final results of the classification, is shown in Fig. 8.

Note that most of the points classified as smooth operating conditions are over the line $\mu_{opt} = \Pi^S$, and the ones classified as rough conditions are exactly on the line $\mu_{opt} = \Pi^R$.

We can also show the same classification results, bounded according to relationship Eq. (43), on the Π^R–Π^S plane, with the isolated gray square (*iv*). Such a projection is presented in Fig. 9. Note that the area spanned by case (*iii*) of the original CFL (sufficient) condition is very small compared to other cases (it contains only about 5% of all cases).

It is also interesting to combine the results from Figs. 8 and 9 in a 3D chart, shown in Fig. 10, with auxiliary planes limiting the possible point locations of the pipeline conditions. The conditions classified as rough lie exactly on the pink surface, therefore we can precisely specify the value of μ_{opt} for these cases. The indefinite (green) class of conditions are subject to the CFL condition ($\mu_{opt} = 1$).

In some approximation, the remaining pipeline working conditions, classified as smooth, require μ_{opt} taken between two planes: blue or bluish (safe option) and the upper limit $\mu_{opt} = 1$ (at the green level). Note that regardless of this, some of the smooth pipeline conditions need exactly $\mu_{opt} = 1$. Nevertheless, in the proposed procedure, when calculating the value of μ_{opt} for any smooth pipe condition, we use the indicated lower boundary. In this way, numerical stability is ensured by a very simple method in all cases of smooth pipeline working conditions.

The complex shape of the optimal μ_{opt} surface for smooth conditions is difficult to precisely describe mathematically based on physical parameters, thus at this stage, we give here only an approximate descrip-
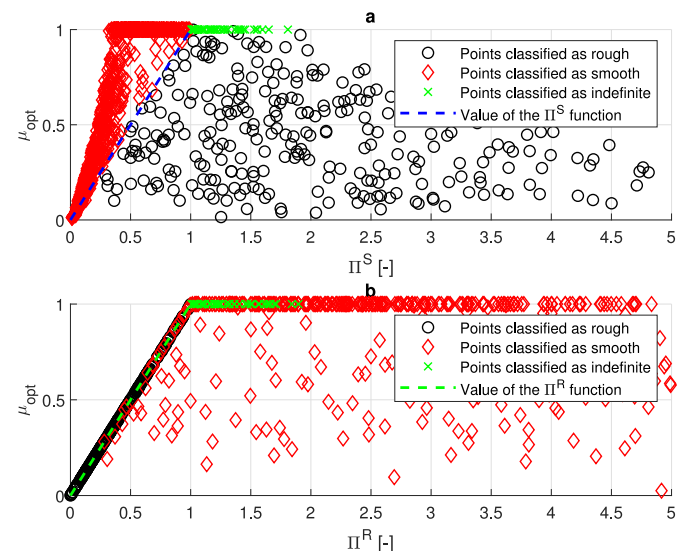

Fig. 7. Procedure for selecting the optimal values of the Courant number. The part denoted as *CFL* refers to the case where the CFL condition is sufficient, and $\overline{CFL}$ denotes the cases where the CFL condition is not sufficient.

Fig. 8. Results of pipeline classifications in terms of functions Π^S (a) and Π^R (b), where the points are classified as smooth (⋄), rough (∘), or indefinite (×). Note that cases (*iv*) representing both smooth and rough conditions are (re)classified to a safer version (smoother or rougher).
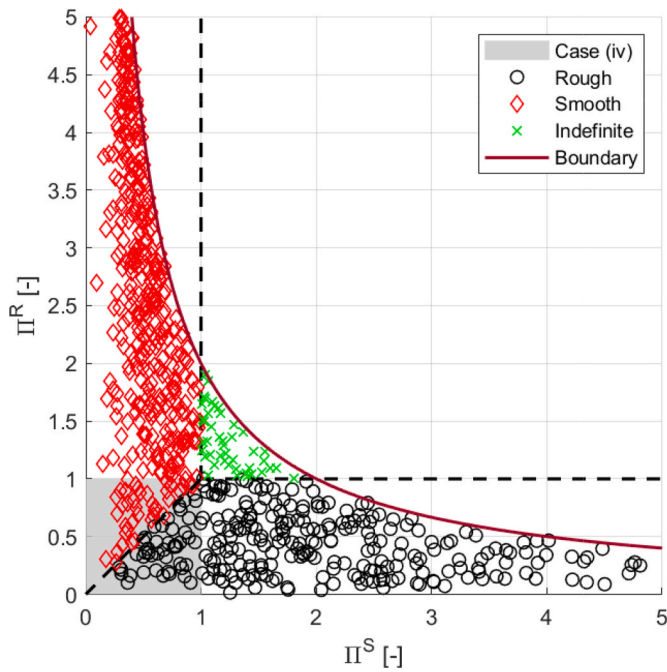
---

[5] A deeper study is necessary to give an even more specific clue (see also Appendix C).

Fig. 9. Results of pipeline classifications on the Π^S–Π^R plane of pipe factors, where points (pipelines) are classified as smooth ($\diamond$), rough ($\circ$) or indefinite ($\times$) conditions. Cases (*iv*) representing smooth-rough pumping conditions are in the gray area. The brown line indicates the upper boundary, limiting the possible arrangement of the pipeline conditions on the Π^S–Π^R plane.
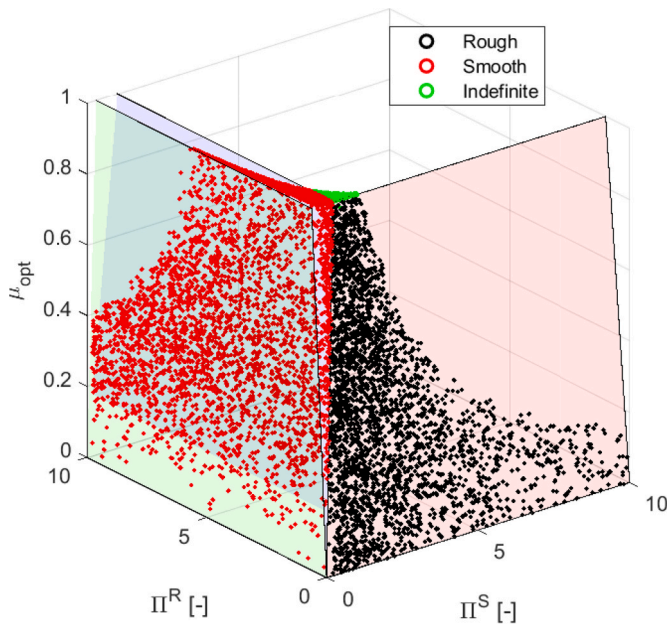

Fig. 10. Courant coefficients for pipeline conditions classified as smooth (red), rough (black), or indefinite (green). The blue (bluish) plane denotes the lower boundary on μ_{opt} for smooth pipe conditions, the pink plane represents the exact values of μ_{opt} for rough conditions and the green piece of a horizontal plane ($\mu_{opt} = 1$) shows the exact upper boundary for the indefinite/CFL pipeline operating conditions.

tion based on some lower (bluish) and upper (greenish) bounding plane. Scatter plots of smooth conditions in terms of Π^S, Π^R and μ_{opt} are presented in Figs. 11–13 using different views.

As shown in Figs. 8 and 12, there are minor anomalies which indicate

the approximate nature of the limiting restriction. However, it was confirmed that the numerical stability is also maintained for these points using the setting $\mu = \Pi^S$.

To verify the above results, we also performed simulations of the flow process based on the μ_{opt} value calculated in accordance with the procedure shown in Fig. 7, for random values of physical flow parameters, represented by the Π factor selected from the ranges described in Table 1. These experiments showed the convergence of all simulations, and thus the correctness of the proposed method. In conclusion, case (*iv*) can also be classified as pressure driven.

This Monte Carlo simulation used to validate the model was an experiment separate from the initial/first Monte Carlo simulation used to analyze the phenomenon and derive the procedure. Thus the first one was used to find the most optimal value of the Courant number (based on the linearized model), while the second Monte Carlo experiment was used to verify the developed procedure (using the nonlinear model).

9. Conclusions

The article has discussed the issue of discretization and numerical stability of systems emulating the flow process. The aggregated state-space model has been derived from the base discrete-time model, which was linearized using an analytically determined steady-state solution.

Two-stage linearization leading to Eq. (22) is a method for calculating the state transition matrix ($\overline{A}_c$) for effective stability analysis using standard numerical means.

The linearization procedure is a key point in our methodology for determining the stability margin, while maximizing the stability margin serves the system's robustness to destabilization as well as its accuracy and convergence speed.

The development proposed in this work leads to an interesting categorization, in which we take into account the technological, mechanical, geometric, physical, mathematical and numerical conditions specific to the process of medium flow in a pipeline. Thanks to the appropriate mathematical modeling, we have obtained a useful model together with the appropriate categorization of such processes that lead to the correct selection of the optimal Courant number and result in
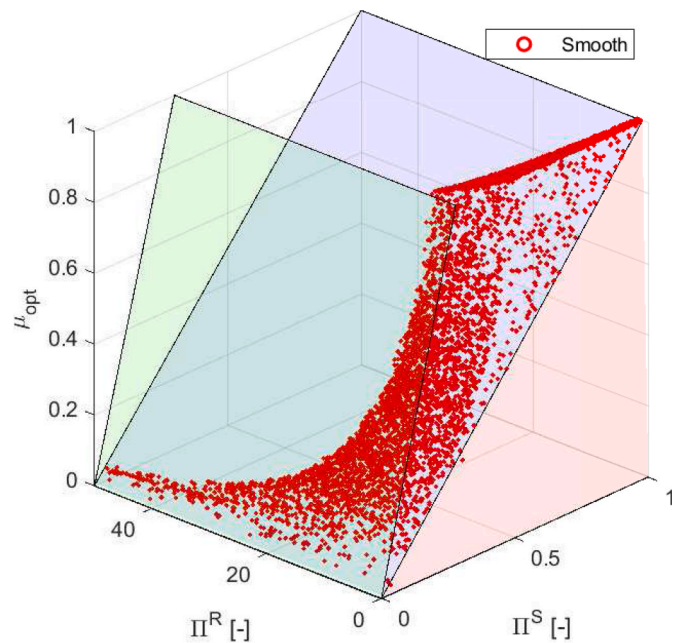

Fig. 11. Distribution of pipeline operating conditions classified as smooth in terms of indexes Π^S and Π^R and μ_{opt}. The blue (bluish) plane means the lower boundary for μ_{opt}, and the green (greenish) plane – the upper boundary.
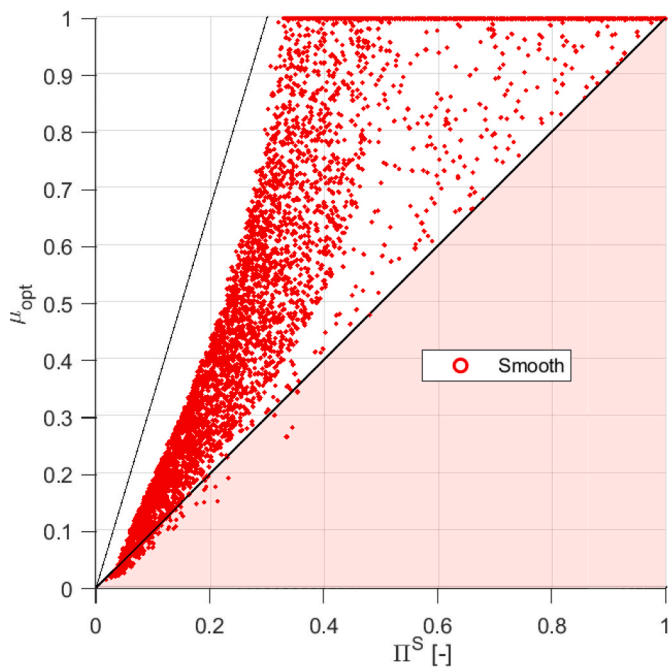
Fig. 12. Distribution of smooth pipeline conditions on the Π^S–μ_{opt} plane with the lower and upper (plane) boundaries represented as two limiting lines.
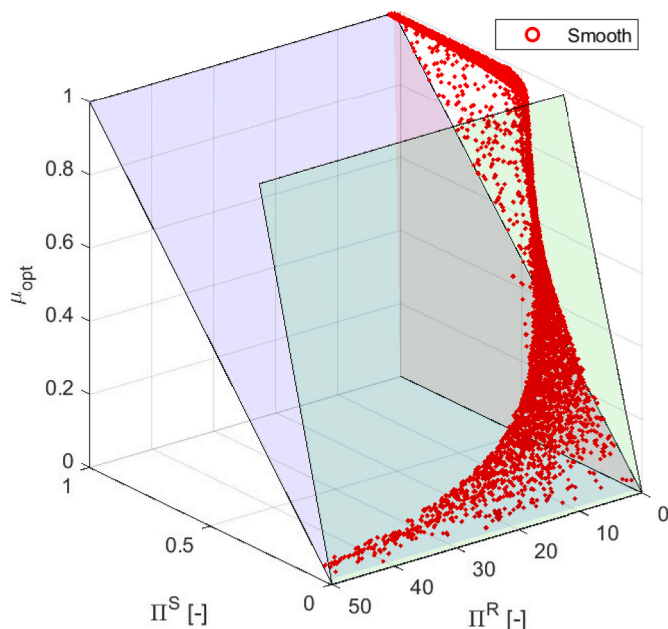

Fig. 13. Distribution of smooth pipeline operating conditions in the Π^S–Π^R–μ_{opt} space, where the lower boundary plane for μ_{opt} is marked as blue/bluish and the upper boundary plane is green/greenish.

suitably conditioned implementations.

The final dichotomous model was derived from the results of the Monte Carlo simulation in which the influence of each parameter (in the full multivariate system) on the optimal Courant number was estimated and consolidated. In this way, taking into account the generally known laws of physics and using numerical methods and mathematical analysis, simple and useful analytical relationships (parameterization) describing the flow process were obtained.

Importantly, the analysis of the relationship between the pipeline operating conditions, Π^R and Π^S, showed an interesting, hyperbolic

limitation of the feasible locations of the modeled pipelines on the Π^R–Π^S plane. Moreover, for the indefinite class of pumping conditions in pipelines (which, however, are only a small subset of the possibilities in the parameter space), it turns out that the CFL condition is (truly) sufficient.

However, in the case of smooth and rough pipeline operating conditions, the CFL condition is insufficient, and other methods of defining the discretization parameters should be used. Parameters of flow mechanics were introduced that allowed us to provide a common formula for dichotomous calculation of μ_{opt}, separately for smooth and rough pipeline operating conditions. The analysis of various sets of pipeline parameters showed that it is difficult to get to the indefinite/CFL region of operating conditions, because it requires the use of an impractical ratio of inlet and outlet pressure. For the practical selection of the Courant number using the formula to calculate μ_{opt}, four possible classes (*i*)-(*iv*) of pipeline operating conditions are distinguished: (*i*) rough, (*ii*) smooth, and (*iii*) indefinite, as well as (*iv*) classified as both smooth and rough. It is surprising that there are three cases where the CFL condition is insufficient.

We must emphasize here the importance of the indirect attribute of the mathematical model of the pipeline, which is its scale. Namely, small scale pipes contribute to the smooth class, while large scale pipes contribute to the rough class. This aspect is evident as the phenomenon of pipe reclassification occurring in the iterative calculation of the optimal Courant number, when the resulting discretization grid converges to the appropriate case. One consequence of analyzing the scale issue is that you should not mis-scale, such as by using short sampling times for long pipelines.

In view of the above, the developed formula Eq. (28), in particular Eq. (33) and Eq. (34), receives an interesting interpretation and application as a technological pipeline classifier. To a large extent, Eq. (28) can also be seen in practice as a balanced stream model. To sum up, Eq. (28) represents the common stream model, technological pipe factor, pipeline classifier and Courant number Eq. (28), different for both smooth and rough cases.

The proposed procedure was numerically verified in simulation tests, which confirmed the correctness and illustrated the usefulness of the obtained results.

9.1. Additional remarks

Modeling the flow process and converting it into a discrete structure is difficult from many points of view. Due to the widespread use of computers for the practical, numerical implementation of such discrete models, the problem of their stability is of the utmost importance.

In general, taking into account, for example, the consequences of limited physics, our project may be subjected to conditions other than those for which it was designed. The complexity of this issue often manifests itself in the sensitivity or instability of the implemented system. In some practical cases, certain empirical rules have been established that must be strictly followed. Nevertheless, a purely theoretical explanation is always welcome as it sheds new light on the field and may even enable new or more efficient applications.

It is interesting that the structure of the state-space model used contains only physical and geometrical parameters, while, for example, the influence of flow velocity is included in the numerical parameters of the state matrix (and dichotomously also in the state vector).

The proposed classification is based on the basic technical pipeline parameters (numerical and mechanical, *i.e.* geometric, and physical). We distinguished smooth working conditions (characterized by a relatively smooth surface, short and wide sections of the pipe, and small numerical scale), rough (with a relatively rough surface, long and narrow sections of the pipe, and large scale), and indefinite ('intermediate' conditions between them, and excluding them).

In addition to the provided convenient mesh selection method for the

numerical implementation of the pipeline flow model upon which the discrete-in-time-and-space computer model is built, the rough operating condition category (*i*) implies the need to spend a significant amount of energy on fluid displacement, while the second operating class (*ii*) requires little effort to push the fluid through the pipeline.

To some extent, our approach to discretization/modeling can be interpreted in accordance with the certainty equivalence principle, as explained in Appendix B.

It should also be noted that the presented analysis was performed for horizontal pipelines (with zero slope angle), which is a widely used assumption that greatly simplifies the considerations (see *e.g.* (Bonzanini et al., 2017)). Other studies (Kowalczuk and Tatara, 2018, 2020) show that inclusion of elevation in the model slightly changes the value of μ_{opt} (for small angles, the impact is small) – of course, outside a small vicinity of the zero mass flow, where the model becomes sensitive to changes in the angle of inclination. However, due to the limited space, this issue has been omitted in this report.

An interesting extension of this work could be the confrontation of our parameterization method with the results of (Konangi et al., 2018) to determine the relationship between the two studies.

Author contribution

Z. Kowalczuk: Conceptualization, Methodology, Formal analysis, Writing – review & editing, Project administration. M.S. Tatara: Investigation, Validation, Visualization, Resources, Software, Writing – original draft.

Declaration of competing interest

The authors declare that they have no known competing financial interests or personal relationships that could have appeared to influence the work reported in this paper.

Appendix A

AFlow Process Matrices

The matrices $\mathbf{A} \in \mathbb{R}^{(N+1)\times(N+1)}$, $\mathbf{B} \in \mathbb{R}^{(N+1)\times(N+1)}$ and $\mathbf{C} \in \mathbb{R}^{(N+1)\times(N+1)}$ of the pipeline flow process model are defined as follows:

$$\mathbf{A} = \left[\begin{array}{c|c} \mathbf{D}_{\frac{N}{2}+1}(c) & \begin{matrix} 2b & 0 & \cdots & 0 & 0 \\ -b & b & \cdots & 0 & 0 \\ \vdots & & \ddots & & \vdots \\ 0 & 0 & \cdots & b & 0 \\ 0 & 0 & \cdots & -b & b \\ 0 & 0 & \cdots & 0 & -2b \end{matrix} \\ \hline \begin{matrix} -b & b & 0 & \cdots & 0 & 0 & 0 \\ 0 & -b & b & \cdots & 0 & 0 & 0 \\ \vdots & & & \ddots & & & \\ 0 & 0 & 0 & \cdots & -b & b & 0 \\ 0 & 0 & 0 & \cdots & 0 & -b & b \end{matrix} & \mathbf{D}_{\frac{N}{2}}(a) \end{array}\right] \tag{44}$$

$$\mathbf{B} = \frac{1}{3}\left[\begin{array}{c|c} \begin{matrix} -c & 0 & \cdots & 0 & 0 \\ 0 & -c & \ddots & 0 & 0 \\ \vdots & & & & \vdots \\ 0 & 0 & \cdots & -c & 0 \\ 0 & 0 & \cdots & 0 & -c \end{matrix} & \mathbf{0}_{\left(\frac{N}{2}+1\right)\times\frac{N}{2}} \\ \hline \mathbf{0}_{\frac{N}{2}\times\left(\frac{N}{2}+1\right)} & \begin{matrix} -a & 0 & \cdots & 0 & 0 \\ 0 & -a & \cdots & 0 & 0 \\ \vdots & & \ddots & & \vdots \\ 0 & 0 & \cdots & -a & 0 \\ 0 & 0 & \cdots & 0 & -a \end{matrix} \end{array}\right] \tag{45}$$

$$\mathbf{C}(\hat{x}^{k-1}) = \left[\begin{array}{ccccc|ccccc} H_0^k & 0 & \cdots & 0 & 0 & -2b & 0 & \cdots & 0 & 0 \\ 0 & H_2^k & \cdots & 0 & 0 & \Gamma_{2+} & \Gamma_{2-} & \ddots & 0 & 0 \\ \vdots & & \ddots & & \vdots & \vdots & & \ddots & & \vdots \\ 0 & 0 & \cdots & H_{N-2}^k & 0 & 0 & 0 & \cdots & \Gamma_{(N-2)+} & \Gamma_{(N-2)-} \\ 0 & 0 & \cdots & 0 & H_N^k & 0 & 0 & \cdots & 0 & +2b \\ \hline b & -b & 0 & \cdots & 0 & \frac{4a}{3} & 0 & \cdots & 0 & 0 \\ 0 & b & -b & \cdots & 0 & 0 & \frac{4a}{3} & \cdots & 0 & 0 \\ \vdots & & \ddots & & \vdots & \vdots & & \ddots & & \vdots \\ 0 & \cdots & b & -b & 0 & 0 & 0 & \cdots & \frac{4a}{3} & 0 \\ 0 & \cdots & 0 & b & -b & 0 & 0 & \cdots & 0 & \frac{4a}{3} \end{array}\right] \tag{46}$$

where $\Gamma_{n\pm} = \frac{Y_n}{2} \pm b$, $H_0^k = \frac{4c}{3} - \frac{\lambda\nu^2\left|\widehat{\overrightarrow{x}}_{(n/2+1)}^k\right|}{2DS^2 u_1^k}$, $H_N^k = \frac{4c}{3} - \frac{\lambda\nu^2\left|\widehat{\overrightarrow{x}}_{(n/2+1)}^k\right|}{2DS^2 u_2^k}$,

$$H_n^k = \frac{4c}{3} - \frac{\lambda\nu^2\left|\widehat{\overrightarrow{x}}_{(n/2+1)}^k\right|}{DS^2\left(\widehat{x}_{(n/2+1+N/2)}^k + \widehat{x}_{(n/2+2+N/2)}^k\right)} \text{ for } n = 2, 4, \ldots, N-2$$

and $\mathbf{D}_W(\theta) \in \mathbb{R}^{W\times W}$ denotes a diagonal matrix with diagonals equal to θ.

And the matrices $\mathbf{D}$ and $\mathbf{E}$ of the model Eq. (10) are given as:

$$\mathbf{D} = \left[\begin{array}{cc} Y_0 + 2b & 0 \\ 0 & 0 \\ \vdots & \vdots \\ 0 & 0 \\ 0 & Y_N - 2b \\ \hline \multicolumn{2}{c}{\mathbf{0}_{\frac{N}{2}\times2}} \end{array}\right] \in \mathbb{R}^{(N+1)\times2}, \quad \mathbf{E} = \left[\begin{array}{cc} 2b & 0 \\ 0 & 0 \\ \vdots & \vdots \\ 0 & 0 \\ 0 & -2b \\ \hline \multicolumn{2}{c}{\mathbf{0}_{\frac{N}{2}\times2}} \end{array}\right] \in \mathbb{R}^{(N+1)\times2} \tag{47}$$

Note that the above principal symbols $\mathbf{A}$, $\mathbf{B}$, $\mathbf{C}$, $\mathbf{D}$ and $\mathbf{E}$ without any subscript refer to the matrices of the base model Eq. (10) of the pipeline flow

process.

BCertainty equivalence and pseudo-time stepping

In control theory, there is the principle of certainty equivalence (CE), which says that the actual values of the state and parameters can be replaced by their estimates when determining the control action. In other words, we assume that the estimates obtain true values of the respective quantities. When the estimates change, the control signal is recalculated, *i.e.* adjusted to current situation (Isermann, 1981). This is also a direct consequence of the separation principle, which states that state observation or identification is independent of the control calculations. CE is also a simplification paradigm that allows us to break down a problem into sub-problems and then compile a complete solution to the overall problem.

Certainly, pseudo-time-stepping can also be interpreted from the CE point of view, since we first estimate the steady state and then perform computational flow calculations assuming the certainty of such an estimate.

It should be noted that the described method can be implemented as adaptive in time (mesh selection) and/or iterative in time (step by step emulation). The adaptive approach, especially in changing conditions (excitations), complies with the CE principle – at each stage, after calculating the steady state (p and q) from the current pressure measurement (p), we can re-estimate the new grid (m_h). Then, treating m_h (or time step Δt itself) as reliable and optimal, we calculate the new steady state, which allows us to re-determine the new optimal mesh. This procedure can be repeated either every time or every few steps.

The next implementation of the CE principle can be seen in the leak detection and isolation (LDI) task. Until leakage occurs, the coefficient of friction is estimated in real-time (this is required because it may change during pipe operation; see, *e.g.* (Wang and Ghidaoui, 2018),). When a leak is detected, the friction value is fixed (*i.e.* we are sure to some extent that this value is true) and used for isolation and identification purposes.

C Discretization grid

The pipeline discretization scheme is shown in Fig. 1, however, it mainly explains the issue of spatial discretization. To describe the dynamics of the object, you also need to consider the mesh parameter and scaling (time or space dimension). In this way, we come to the total discretization grid, which is illustrated in Fig. 14.
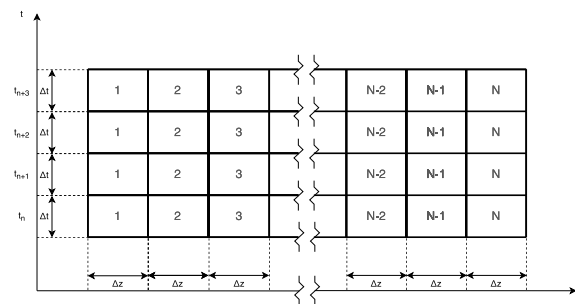

Fig. 14. Visualization of the discretization grid.

In the grid of Fig. 14, the most important element is the relationship between the steps of time and space, which is represented by the slope of the dotted-blue line[6] shown in Fig. 15. The slope corresponds to grid parameter m_h. It is clear that thinking about spatial discretization Δz lower than Δz_s is not rational, because in time equal to Δt information will jump by this distance quantum ($\Delta z_s = \nu \Delta t$).
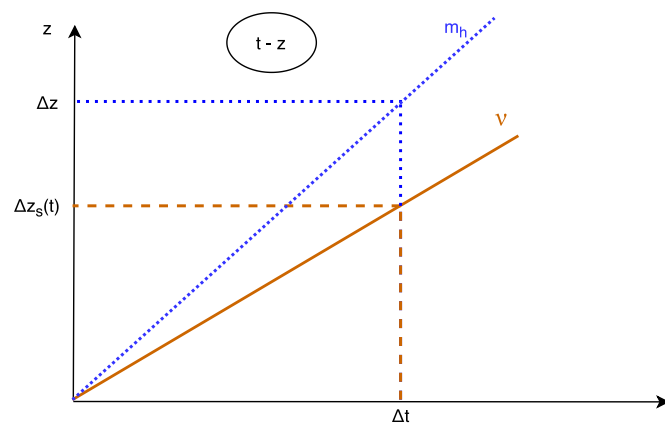

Fig. 15. The limit quantum of information distance applicable at the time step is associated with the surrogate speed of sound propagation. Above line ν is the allowed region for the grid parameters (m_h), as shown by the dotted-blue lines.

By imposing the CFL condition on the presented graph, we get the angle (pencil of the line) representing the permissive discretization grids lying

---

[6] In the adaptive case, the line may be represented by a polyline with a variable slope.

below the boundary line corresponding to the Courant number equal to 1, as well as the region excluded due to the CFL criterion. Such circumstances are visualized in Fig. 16, where the (differently described) plane $t - z$ is used.
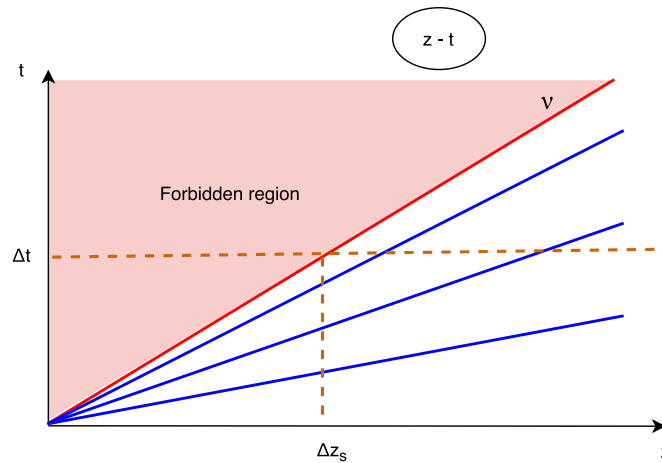

Fig. 16. Discretization grid with a natural interpretation of CFL. The shaded region contains values in which $\nu \Delta t / \Delta z > 1$ (*i.e.* when the CFL criterion is not met).

The excluded area results from the fact that spatial discretization does not allow the dynamics of changes in the information observed to be captured. Because time is an abstract and artificial quantity here, the reasoning proposed relates to spatial discretization. From a practical point of view and taking into account the surrogate speed of sound, we can say that for Δz lower than Δz_s, the insertion of a measuring point in a segment of this length is pointless, because in the time between two successive computational steps the information flies over such a segment and therefore is not measurable in it. Therefore, the forbidden region does not allow the effect of information transfer. We can imagine this as a gap between seeing and hearing lightning (because light travels faster than sound), or as a discrepancy between seeing and hearing an airplane. On the other hand, the lines below the boundary line are suitable to represent the optimal mesh matched to the detailed experimental settings (technological flow conditions).

In may be interesting to consider the following example: the length of the designed pipe is $L = 30$ km, the (surrogate) speed of sound is $\nu = 341 \frac{m}{s}$, the sampling time is $\Delta t = 200$ ms, and according to the given formula, we calculated $\mu_{opt} = 0.134$. In this way, we can specify the spatial step Δz as $\Delta z = \frac{\Delta t \nu}{\mu_{opt}}$, which gives $\Delta z \approx 508.95$ m. Because the pipeline should be divided into an even number of N sections, spatial step Δz must be rounded up, observing the CFL condition (see Fig. 16). In other words, it is best if the adopted Δz is greater than the calculated one and divides the pipeline (L) into an even integer number of segments. In this example, taking $N = 58$, the spatial step can be set to $\Delta z = \frac{30000}{58} = 517.24$ [m].

Note that you are not required to use a fixed value of m_h. However, we provide a formula for quickly calculating the value of m_h in any step based on the latest data. The proposed procedure implements the methodology for determining the optimal stability margin, *i.e.* it makes the simulation the most resistant to destabilization.

Several sample pipelines were analyzed to show how the value of μ_{opt} changes in subsequent iterations of the process of recalculation of Δz, which, due to its entangled nature, requires repeated use of the same data to calculate the optimal μ_{opt}. The parameters of these pipes are shown in Table 3, while the results of the iterative calculation of the number of segments and coefficient μ_{opt} along with the categorization of pipes (*i*)-(*iv*) are shown in Fig. 17. To fine-tune the procedure of Fig. 7, in the case of (*iv*), Courant number μ_{opt} was determined based on the average value of the two pipe factors (smooth and rough).

Table 3
Parameters of the sample pipelines.

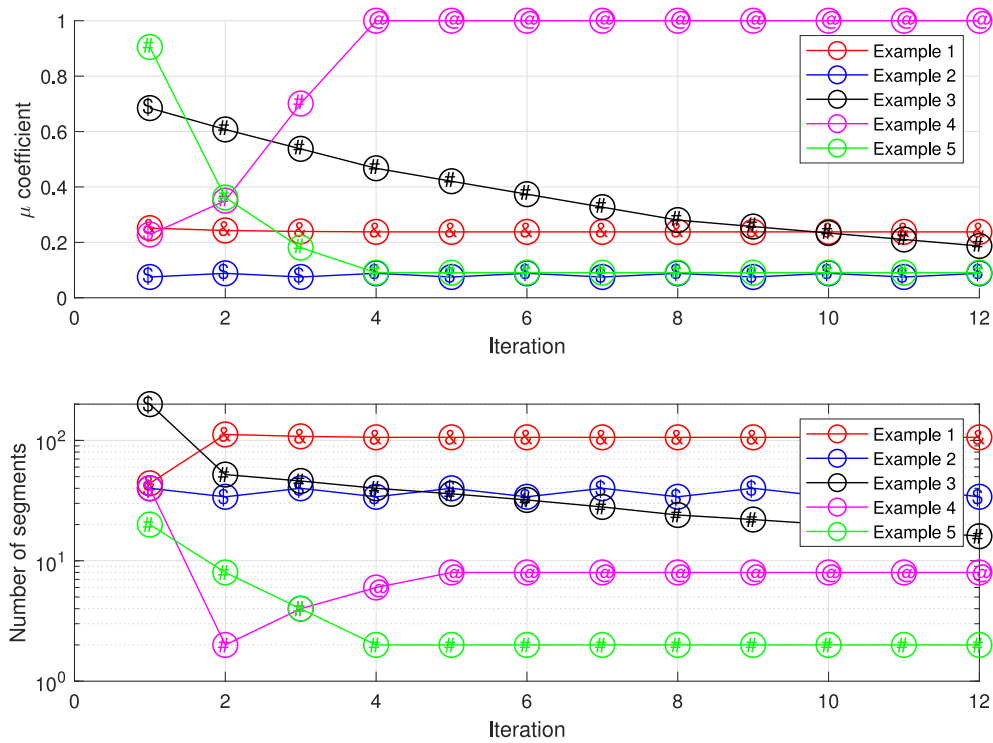|	Example 1	Example 2	Example 3	Example 4	Example 5
Length [km]	30	30	5000	500	500
Diameter [m]	0.5	0.5	0.4	0.6	0.4
Friction coefficient [-]	0.018	0.0018	0.03	0.002	0.02
Initial number **of segments**	44	40	200	40	20
Inlet pressure [bar]	80	20	15	15	15
Outlet pressure [bar]	1	10	10	10	10
Sampling time [s]	0.2	0.2	200	200	200

Fig. 17. Examples of the evolution of the optimal Courant number μ_{opt} and the optimal number of segments in subsequent iterations; with the categorization of the pipe marked as (#) for rough class (*i*), ($) – smooth class (*ii*), (@) – indefinite case (*iii*), (&) variant (*iv*).

This graph shows that sometimes it takes a few iterations to find the optimal value of μ_{opt} (we recommend 10–20 iterations). In examples 1–2 (short pipes, small scale), we use small sampling times, while in examples 3–5 (long pipes, large scale) we consider relatively large sampling times. Small scale pipelines tend to remain in the smooth cases (*ii*) or (*iv*) (with a small μ_{opt} and a medium or large number of segments N). In turn, large scale pipes consistently converge to the other two distinguished cases (*i*) (with a small μ_{opt} and a medium or low N) or (*iii*) (the CFL case with a high μ_{opt} and a medium N). We can also observe intriguing patterns when reclassifying pipes related to the selected sampling time scale. In Fig. 17 we can see, for example, that Example 4, initially assigned to the (wrong) smooth type (*ii*), is temporarily reclassified to the rough class (*i*), and then converts to a stable indefinite case (*iii*) (the CFL, neither smooth nor rough).

At this stage of the research, we can conclude that for small scale pipes, the appropriate (ultimate) class should generally be smooth (*ii*) (or in particular (*iv*)), while for large scale pipes – rough (*i*) or indefinite/CFL (*iii*). Therefore, it seems that the common variant (*iv*) is more strongly associated[7] with the smooth class (*ii*). Moreover, at all costs, you should not enter mis-scaling,[8] such as using a short sampling time for long pipelines. However, further analysis of this problem is needed.

In addition to the aforementioned recalculation of the spatial discretization step, in some situations (systems), it is possible to manipulate the sampling time. If possible, calculating the optimal Courant number while changing the sampling time will not reclassify the pipe, but may change the scale of the problem. Consider the following example: the length of the designed pipe is $L = 30$ km, the surrogate speed of sound is $\nu = 341\frac{m}{s}$, the space step is $\Delta z = 1$ km and according to the formula given, we calculate $\mu_{opt} = 0.134$. In this way, we can specify the time interval as $\Delta t = \frac{\Delta z \mu_{opt}}{\nu}$, which gives $\Delta t \approx 392.96$ ms. As a result of quantization (Kowalczuk, 1989), sometimes only some discrete values of the sampling time can be set, then the obtained value should be rounded down, observing the CFL condition (see Fig. 16).

D Emulation procedure

To clarify the proposed methodology in a practical algorithmic form, we present a useful emulation procedure below. It is based on input data in the form of the pressure and mass flow rate measured at both ends of a pipe. As a result of processing, we obtain a complete pressure distribution and mass flow rate along the entire pipe. In addition, friction coefficient and leak detection data can be estimated in the target LDI procedure.

Step 0. Initialize the time index and all known parameters: length, diameter, surrogate speed of fluid sound, desired number of segments, as well as the coefficient of friction.[9]

Step 1. Measure the inlet and outlet pressures and mass flow rates, and enter them into the model.

Step 2. (**CFL part**) Check if the measured pressure changed significantly (with respect to previous iteration). If yes, recalculate the optimal time

---

[7] This relationship is due to the fact that cases (*ii*) and (*iv*) take place for small scale pipelines.
[8] Compare the parameterization of the examples described in Table 3.
[9] The friction coefficient can be assessed initially from the pipe documentation and fluid parameters (Kowalczuk and Tatara, 2020).

step and compare it[10] with the system sampling period.[11] Otherwise, use the previous value of the time step.

Step 3. Calculate the steady state conditions (flow and pressure) as well as the *a priori* state vector itself.

Step 4. Calculate fixed-value matrix $\mathbf{A}_c$ in the proximity of the operating point, and then calculate the state vector estimate at the given time (including local pressures and mass flow rates).

Various extensions are possible. In the case of LDI, these can be the next two steps:

Step 5. Perform the procedure for estimating the friction coefficient.[12]

Step 6. Run a detection algorithm to check for leaks.

Step 7. Only if a leak is detected, go into isolation and leak identification mode.

Step 8. Update the time index and go to **Step 1**.

This closes the entire LDI procedure, without going into further detail. Note that the presented algorithm fits within the adaptive framework. It may also be designed for pseudo-time-stepping to a steady state, i.e. for iteratively implementing locally optimized pseudo-time steps.

The matrix $\mathbf{A}_c$ is linearized around the operating point associated with the predicted local steady state. We assume that this value is sufficiently accurate to obtain the proper linearization effect of the matrix in the vicinity of this steady state. This, in turn, allows us to provide a simple analytic model that can be analyzed using standard numerical tools.

E Glossary

In Table 4 the most important nomenclature used throughout the paper is collected and discussed.

Table 4
Glossary of the most important terms with explanations.

Term	Meaning
Optimal Courant number	The μ coefficient that assures the maximal stability margin
Critical Courant number	The μ coefficient for which the considered model becomes unstable
Maximum stability margin	The distance from the unit circle of the maximal eigenvalue of the state transition matrix (positive if the eigenvalue is inside the circle, negative if it is outside)
Pumping conditions	Either rough, smooth or indefinite region of operation

References

Alghurabi, A., Mohyaldinn, M., Jufar, S., Younis, O., Abduljabbar, A., Azuwan, M., 2020. Cfd numerical simulation of standalone sand screen erosion due to gas-sand flow. J. Nat. Gas Sci. Eng. 103706. https://doi.org/10.1016/j.jngse.2020.103706. http://www.sciencedirect.com/science/article/pii/S1875510020305606.

Bauer, A.L., Loubère, R., Wendroff, B., 2008. On stability of staggered schemes. SIAM J. Numer. Anal. 46, 996–1011. https://doi.org/10.1137/060660151 doi:10.1137/060660151.

Billmann, L., Isermann, R., 1987. Leak detection methods for pipelines. Automatica 23, 381–385.

Bonzanini, A., Picchi, D., Poesio, P., 2017. Simplified 1D incompressible two-fluid model with artificial diffusion for slug flow capturing in horizontal and nearly horizontal pipes. Energies 10, 1372. http://www.mdpi.com/1996-1073/10/9/1372. doi:10.3390/en10091372.

Bridson, R., 2015. Fluid Simulation for Computer Graphics, second ed. CRC Press.

Brogan, W., 1991. Modern Control Theory, third ed. Prentice Hall.

Capuano, F., Mastellone, A., Angelis, E.D., 2017. A conservative overlap method for multi-block parallelization of compact finite-volume schemes. Comput. Fluids 159, 327–337. https://doi.org/10.1016/j.compfluid.2017.10.017. http://www.sciencedirect.com/science/article/pii/S0045793017303742.

Chen, Z., Zhang, J., 2001. An unconditionally stable 3-D ADI-MRTD method free of the CFL stability condition. IEEE Microw. Wireless Compon. Lett. 11, 349–351. https://doi.org/10.1109/7260.941786. http://ieeexplore.ieee.org/document/941786/.

Courant, R., Friedrichs, K., Lewy, H., 1967. On the partial difference equations of mathematical physics. IBM J. Res. Dev. 11, 215–234. http://ieeexplore.ieee.org/document/5391985/. doi:10.1147/rd.112.0215, arXiv:AD0832715.

Czernous, W., 2008. Numerical method of characteristics for semilinear partial functional differential systems. J. Numer. Math. 16, 1–21. https://doi.org/10.1515/JNUM.2008.001 doi:10.1515/jnum.2008.001.

Decuyper, J., De Troyer, T., Runacres, M., Tiels, K., Schoukens, J., 2018. Nonlinear state-space modelling of the kinematics of an oscillating circular cylinder in a fluid flow. Mech. Syst. Signal Process. 98, 209–230. https://doi.org/10.1016/j.ymssp.2017.04.048. http://www.sciencedirect.com/science/article/pii/S0888327017304255.

Duquette, J., Rowe, A., Wild, P., 2016. Thermal performance of a steady state physical pipe model for simulating district heating grids with variable flow. Appl. Energy

178, 383–393. https://www.sciencedirect.com/science/article/pii/S0306261916308662. doi:10.1016/J.APENERGY.2016.06.092.

Gordner, A., Wittum, G., 2007. Low Machnumber aeroacoustics – a direct one-grid approach. J. Numer. Math. 15 https://doi.org/10.1515/jnma.2007.007 doi:10.1515/jnma.2007.007.

Gunawickrama, K., 2001. Leak Detection Methods for Transmission Pipelines. Ph.D. thesis. Gdansk University of Technology, Gdansk, Poland.

Hafsi, Z., Elaoud, S., Mishra, M., 2019. A computational modelling of natural gas flow in looped network: effect of upstream hydrogen injection on the structural integrity of gas pipelines. J. Nat. Gas Sci. Eng. 64, 107–117. https://doi.org/10.1016/j.jngse.2019.01.021. http://www.sciencedirect.com/science/article/pii/S1875510019300290.

Hamming, R.W., 1986. Numerical Methods for Scientists and Engineers. Dover Publications, USA.

Hibbitt, H., Becker, E., Taylor, L., 1979. Nonlinear analysis of some slender pipelines. Comput. Methods Appl. Mech. Eng. 17–18, 203–225. https://doi.org/10.1016/0045-7825(79)90088-4. http://www.sciencedirect.com/science/article/pii/0045782579900884.

Isermann, R., 1981. Digital Control Systems. Springer Verlag Berlin Heidelberg GmbH.

Konangi, S., Palakurthi, N.K., Ghia, U., 2018. Von Neumann stability analysis of first-order accurate discretization schemes for one-dimensional (1D) and two-dimensional (2D) fluid flow equations. Comput. Math. Appl. 75, 643–665. https://doi.org/10.1016/j.camwa.2017.09.040. http://www.sciencedirect.com/science/article/pii/S089812211730620X.

Kornhaas, M., Schäfer, M., Sternel, D.C., 2015. Efficient numerical simulation of aeroacoustics for low mach number flows interacting with structures. Comput. Mech. 55, 1143–1154. https://doi.org/10.1007/s00466-014-1114-1 doi:10.1007/s00466-014-1114-1.

Kowalczuk, Z., 1989. Finite register length issue in the digital implementation of discrete PID algorithms. Automatica 25, 393–405.

Kowalczuk, Z., Tatara, M., 2016. Approximate models and parameter analysis of the flow process in transmission pipelines. In: Advanced and Intelligent Computations in Diagnosis and Control. Springer, Cham, pp. 239–252. http://link.springer.com/10.1007/978-3-319-23180-8_17. doi:10.1007/978-3-319-23180-8_17.

Kowalczuk, Z., Tatara, M., 2017. Numerical issues and approximated models for the diagnosis of transmission pipelines. In: Modeling and Monitoring of Pipelines and Networks: Advanced Tools for Automatic Monitoring and Supervision of Pipelines. Springer, Cham, pp. 39–62. http://link.springer.com/10.1007/978-3-319-55944-5_3. doi:10.1007/978-3-319-55944-5_3.

---

[10] You may need to negotiate this with the operating system.

[11] When using a fixed mesh parameter (in time and space), called uniform (Hamming, 1986; Sharma, 2016), the optimal determination of this parameter, including the time step, is done only once.

[12] According to the adopted formula, see *e.g.* (Kowalczuk and Tatara, 2020).

Kowalczuk, Z., Tatara, M., 2018. Analytical steady-state model of the pipeline flow process. In: 23rd Intl Conference on Methods and Models in Automation and Robotics. IEEE, Szczecin, pp. 182–187.

Kowalczuk, Z., Tatara, M., Stefański, T., 2018. Reduction of computational complexity in simulations of the flow process in transmission pipelines. In: Kościelny, J.M., Syfert, M., Sztyber, A. (Eds.), Advanced Solutions in Diagnostics and Fault Tolerant Control. Springer International Publishing, Cham, pp. 241–252.

Kowalczuk, Z., Tatara, M.S., 2020. Improved model of isothermal and incompressible fluid flow in pipelines versus the Darcy–weisbach equation and the issue of friction factor. J. Fluid Mech. 891 https://doi.org/10.1017/jfm.2020.131. A5.1–26.

Lax, P.D., Richtmyer, R.D., 1956. Survey of the stability of linear finite difference equations. Commun. Pure Appl. Math. 9, 267–293. https://doi.org/10.1002/cpa.3160090206. https://onlinelibrary.wiley.com/doi/abs/10.1002/cpa.3160090206. arXiv.

Morton, K.W., Mayers, D.F., 2005. Numerical Solution of Partial Differential Equations: an Introduction, 2 ed. Cambridge University Press. https://doi.org/10.1017/CBO9780511812248.

Namiki, T., Ito, K., 1999. A new FDTD algorithm free from the CFL condition restraint for a 2D-TE wave. In: IEEE Antennas and Propagation Society International Symposium. 1999 Digest. (USNC/URSI National Radio Science Meeting, Cat. No.99CH37010). IEEE, pp. 192–195. http://ieeexplore.ieee.org/document/789114/. doi:10.1109/APS.1999.789114.

Shao, W., Li, J., 2018. Three time integration methods for incompressible flows with discontinuous Galerkin Boltzmann method. Comput. Math. Appl. 75, 4091–4106. https://doi.org/10.1016/j.camwa.2018.03.015. http://www.sciencedirect.com/science/article/pii/S0898122118301445.

Sharma, A., 2016. Introduction to Computational Fluid Dynamics. John Wiley & Sons.

Stefański, T., Drysdale, T.D., 2008. Parallel ADI-BOR-FDTD algorithm. IEEE Microw. Wireless Compon. Lett. 18, 722–724. https://doi.org/10.1109/LMWC.2008.2005216.

Thanh, M.D., 2014. Building fast well-balanced two-stage numerical schemes for a model of two-phase flows. Commun. Nonlinear Sci. Numer. Simulat. 19, 1836–1858. https://doi.org/10.1016/j.cnsns.2013.10.017. http://www.sciencedirect.com/science/article/pii/S1007570413005066.

Thomas, J.W., 1995. Numerical Partial Differential Equations: Finite Difference Methods, 22. Springer, New York, NY. https://doi.org/10.1007/978-1-4899-7278-1 of Texts in Applied Mathematics.

Wang, P., Ho, M.T., Wu, L., Guo, Z., Zhang, Y., 2018. A comparative study of discrete velocity methods for low-speed rarefied gas flows. Comput. Fluids 161, 33–46. https://doi.org/10.1016/j.compfluid.2017.11.006. http://www.sciencedirect.com/science/article/pii/S0045793017304140.

Wang, X., Ghidaoui, M.S., 2018. Identification of multiple leaks in pipeline: linearized model, maximum likelihood, and super-resolution localization. Mech. Syst. Signal Process. 107, 529–548. https://doi.org/10.1016/j.ymssp.2018.01.042. http://www.sciencedirect.com/science/article/pii/S0888327018300505.

White, F., 2011. Fluid Mechanics. McGraw-Hill series in mechanical engineering, McGraw Hill. URL: https://books.google.pl/books?id=egk8SQAACAAJ.

Woodward, P., Colella, P., 1984. The numerical simulation of two-dimensional fluid flow with strong shocks. J. Comput. Phys. 54, 115–173. https://doi.org/10.1016/0021-9991(84)90142-6. https://www.sciencedirect.com/science/article/pii/0021999184901426.

Yeung, P.K., Sreenivasan, K.R., Pope, S.B., 2018. Effects of finite spatial and temporal resolution in direct numerical simulations of incompressible isotropic turbulence. Physical Review Fluids 3, 064603. https://doi.org/10.1103/PhysRevFluids.3.064603. https://link.aps.org/doi/10.1103/PhysRevFluids.3.064603.
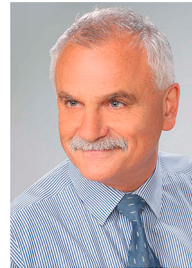
Zdzisław Kowalczuk – Prof. DSc PhD MScEE (2003, 1993, 1986, 1978). Since 1978 he has been with the Faculty of Electronics, Telecommunications and Informatics at the Gdańsk University of Technology, where he is a Full Professor in automatic control and robotics, and the Chair of the Department of Robotics and Decision Systems. He held visiting appointments at University of Oulu (1985), Australian National University (1987), Technische Hochschule Darmstadt (1989), and at George Mason University (1990–1991). Main scientific interests include robotics, control theory, adaptation, system modeling, identification and estimation, diagnostics, failure detection, signal processing, artificial intelligence, control engineering and computer science. He has authored and co-authored over 20 books (incl. WNT, 2002; Springer, 2004–2016, PWNT, 2007–2019), about 120 journal papers (45 on JCR) and over 300 conference publications and book chapters. His citation index on Google Scholar exceeded 25 hundreds. He has also over 750 JCR quotes and his Hirsch indexes range from 10 to 18. He is the President of the Polish Consultants Society (TKP) and of the Polish Society for Measurements, Automatic Control and Robotics (POLSPAR, the NMO of IFAC), and a member of the Automation and Robotics Committee of the Polish Academy of Sciences. Since 2003 professor Kowalczuk is the founder and chief editor of the publishing house PWNT – the Pomeranian Science and Technology Publishers. He is also a recipient of 1990 and 2003 Research Excellence Awards of Polish National Education Ministry, and the 1999 Polish National Science Foundation Award in automatic control, as well as the 2014 Medal of the Association of Polish Electrical Engineers SEP named after Professor Paweł Jan Nowacki.

Marek S. Tatara PhD – MSc was born in 1991 in Olsztyn, Poland. Achieved his PhD in 2019 from the Gdańsk University of Technology in the field of Automatic Control, Electronics and Electrical Engineering. His scientific interests concern mathematical modeling of physical processes, diagnostics, signal processing applied to industrial processes, and evolutionary music composition. Member of Polish Society for Measurement, Automatic Control and Robotics, Vice-chair of the Technical Committee TC 7.5. Intelligent Autonomous Vehicles on Social Media of International Federation of Automatic Control. Currently works as Assistant Professor at the Gdańsk University of Technology and Chief Scientific Officer at DAC.digital.